

Non-contact excitation of multi-GHz lithium niobate electromechanical resonators

Danqing Wang^{1,†}, Jiacheng Xie^{1,†}, Yu Guo¹, Mohan Shen¹, Hong X. Tang^{1,*}

¹*Department of Electrical Engineering, Yale University,
New Haven, Connecticut 06511, USA*

**hong.tang@yale.edu*

[†]*Authors contribute equally*

(Dated: 2024-07-09)

The demand for high-performance electromechanical resonators is ever-growing across diverse applications, ranging from sensing and time-keeping to advanced communication devices. Among the electromechanical materials being explored, thin-film lithium niobate stands out for its strong piezoelectric properties and low acoustic loss. However, in nearly all existing lithium niobate electromechanical devices, the configuration is such that the electrodes are in direct contact with the mechanical resonator. This configuration introduces an undesirable mass-loading effect, giving rise to spurious modes and additional damping. Here, we present an electromechanical platform that mitigates this challenge by leveraging a flip-chip bonding technique to separate the electrodes from the mechanical resonator. By offloading the electrodes from the resonator, our approach yields a substantial increase in the quality factor of these resonators, paving the way for enhanced performance and reliability for their device applications.

INTRODUCTION

Electromechanical resonators are at the core of many resonator technologies, particularly in communication applications. The advent of fifth-generation (5G) networks has heightened the demand for high-performance electromechanical resonators [1]. High frequency resonators in the upper microwave and millimeter-wave bands offer expansive bandwidths for high-data-rate communications. However, the substantial insertion loss at these frequencies presents challenges for scaling electromechanical resonators to operate within this range. Hence, there is a critical need to devise high-frequency, low-loss resonators to address this challenge effectively.

Among various material platforms of micro-electromechanical systems (MEMS), thin-film lithium niobate (TFLN) has attracted significant attention thanks to its excellent piezoelectric properties [2], low acoustic loss [3], and compatibility with large-wafer thin-film processing. Recently, large electromechanical coupling has been reported with *z*-cut TFLN lamb wave modes [4]. Moreover, sub-THz TFLN electromechanical resonators have also been demonstrated [5], showcasing the potential of such a platform for broadband applications. To further enhance TFLN resonators for RF filter applications and quantum phononics research, considerable efforts have been dedicated to improving the quality factor (*Q*) of devices, including reducing surface roughness of TFLN [6], optimizing the release process [7], and modifying the design and materials of coupling electrodes [7–9]. However, in all these implementations, the metal electrodes are directly in contact with the lithium niobate (LN) membranes, which leads to significant mechanical losses in the electromechanical systems [10–13].

The substantial loss accompanied by the contact elec-

trodes motivates researchers to develop mechanical resonators excited through non-contact electrodes. Ref. [14] employed capacitive-piezoelectric aluminum nitride (AlN) lamb wave resonators to showcase the *Q* enhancement of the non-contact configuration at around 1 GHz. In this paper, we experimentally demonstrate a non-contact TFLN electromechanical platform that can operate up to around 30 GHz. By employing a flip-chip bonding approach, we achieve separation of the electrodes from the resonator body through an air gap, resulting in effectively reduction of mechanical losses and suppression of spurious modes. We propose that by further reducing the gap between electrodes and the membrane to a nanometer scale, we could still achieve a notable enhancement of the device quality factor meanwhile maintaining a large electromechanical coupling strength.

DEVICE DESIGN AND FABRICATION

As depicted in Fig. 1, panel (a) illustrates the conventional configuration where the electrodes make direct contact with the LN membrane, while panel (b) outlines our proposed scheme where an air gap is introduced between the electrodes and the membrane. In these configurations, a horizontal electric field is utilized to couple to the *z*-cut TFLN thickness-shear (TS) modes [5] through the large e_{51} piezoelectric coupling element. These thickness modes, bounded by the free top and bottom surfaces of the membrane, have a near-dispersionless characteristic where the mechanical resonant frequency f , mode order m , film thickness h , and acoustic velocity v are related by $mv = 2hf$.

In the direct-contact system, acoustic waves inevitably propagate into the electrodes, as indicated by the displacement field u in Fig. 1(c-i). Consequently, the electrodes provide a dissipation path for the mechanical en-

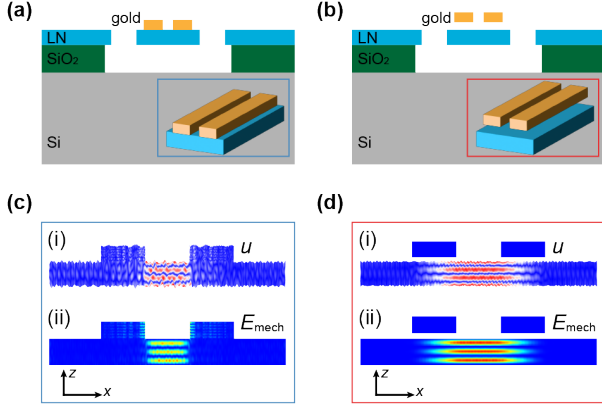


FIG. 1. Schematics of direct-contact and non-contact LN electromechanical resonators. (a) Gold electrodes in direct contact with the LN membrane. (b) Electrodes suspended over the LN membrane. Insets of (a)(b) show three-dimensional perspectives of the central region of electromechanical resonators. (c)(d) Simulated on-resonance displacement field (i) and mechanical energy distribution (ii) of the third-order TS mode (TS-3). Color from blue to red maps the displacement amplitude and stored energy from minimum to maximum.

ergy E_{mech} as shown in Fig. 1(c-ii). In this scenario, mechanical damping associated with the electrodes contributes to the overall decay of the stored energy in the electromechanical resonator. In contrast, the non-contact platform circumvents this issue by fully confining the acoustic energy in the LN membrane, leveraging the significant mechanical impedance mismatch between the solid and the air. This confinement is visualized through the displacement field and the energy distribution in Fig. 1(d-i, ii).

Loss mechanism inside an electromechanical resonator can be quantitatively described by an energy participation ratio model:

$$\frac{1}{Q_{\text{sys}}} = \sum p_i \eta_i \approx p_m \eta_m + p_e \eta_e \quad (1)$$

where Q_{sys} is the mechanical quality factor of the whole system, η_i is the loss factor [15] of each loss channel and $p_i = E_i/E_{\text{total}}$ is the energy participation ratio of each channel. Here, we focus on the loss induced by the LN membrane (loss factor η_m), including LN's intrinsic damping and the anchor loss, and the loss associated with the gold electrodes (loss factor η_e). In the non-contact scenario, the mechanical energy confined in the TFLN membrane is dominant while p_e is negligible, which contributes to a high quality factor. To validate the advantage of the non-contact platform numerically, we perform finite-element method (FEM)-based simulations (COMSOL) to verify its Q-enhancement. As for the damping parameters used in the simulations, we choose

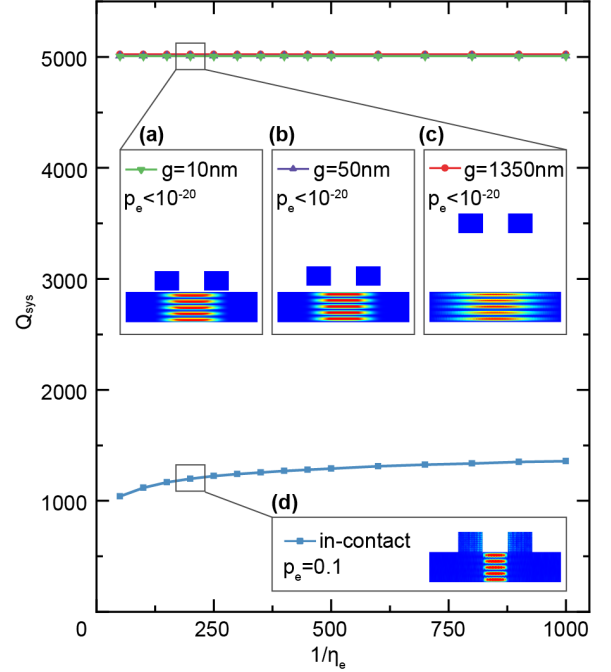


FIG. 2. Simulated system Q versus assumed gold loss factor η_e . The blue line represents the direct-contact case, while the green, purple, and red lines depict non-contact case with air gaps of 10 nm, 50 nm and 1350 nm, respectively. Simulations are based on the TS-5 mode of 300 nm TFLN with 200 nm gold electrodes, and Q is fitted using a multi-resonance mBVD model. (a-d) display each configuration's energy distribution and participation ratio at $\eta_e=1/200$.

a realistic value of $1/5000$ as η_m for the TFLN, based on the extracted data from a LN acoustic delay line [16]. Considering that there is no unified value of the gold loss factor, we sweep across a broad range of η_e ($1/50$ to $1/1000$ [13, 17, 18]) to validate the superiority of the non-contact platform in all these scenarios. The corresponding system Q of the fifth-order TS mode (TS-5) at 30 GHz is shown in Fig. 2, for four different configurations: (a) 10 nm air gap (g); (b) 50 nm air gap; (c) 1350 nm air gap; (d) electrodes in contact with the membrane. In the direct-contact device, gold electrodes will vibrate with the LN membrane, as shown in Fig. 2(d). For all loss factor η_e considered, the energy participation ratio of the electrodes (p_e) ranges from 4% to 40%, which is a limiting factor of the mechanical Q of the system. Moreover, spurious modes introduced by electrodes broaden the resonant spectrum, leading to a decrease in the observed system Q. However, in the non-contact platform, as shown in Fig. 2(a-c), the air gap prevents acoustic waves from propagating into the electrodes, resulting in a significantly reduced p_e (less than 10^{-20} , obtained from simulation), and the system Q is close to the intrinsic value of the LN, regardless of the size of the air

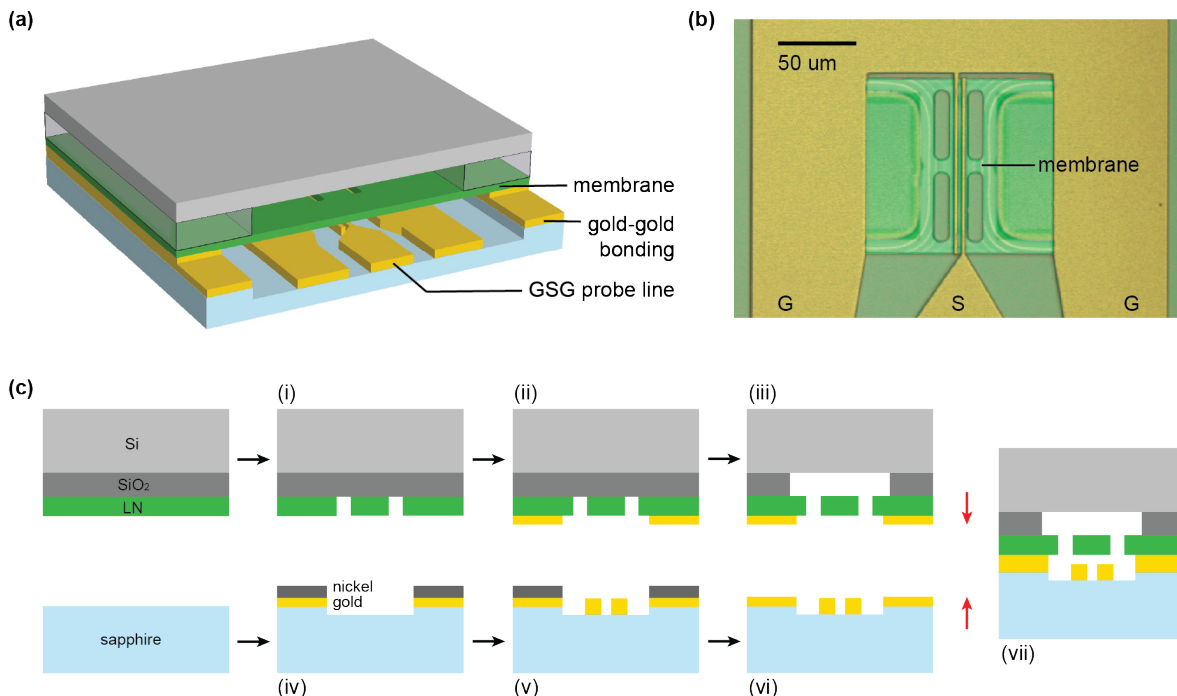


FIG. 3. (a) Schematic of a flip-chip bonded non-contact resonator (not to scale). (b) Optical microscope image of a device, viewed from the top electrode side. The width of the membrane is $16\ \mu\text{m}$ and the length is $140\ \mu\text{m}$. (c) Fabrication flow: (i) LN is etched by Ar ion milling. (ii) gold is deposited at the bonding area. (iii) SiO_2 buffer layer is removed in BOE and the chip is dried in CPD. (iv) gold and nickel are deposited at the bonding area of the sapphire chip, and the remaining area is etched around $150\ \text{nm}$. (v) $200\ \text{nm}$ -thick gold electrodes are deposited. (vi) nickel is removed. (vii) two chips are bonded.

gap, demonstrating advantages over the direct-contact platform.

We employ a flip-chip bonding technique to realize a narrow air gap between the TFLN membrane and the electrodes. The complete resonator construction is depicted in Fig. 3(a), where a sapphire chip with metal electrodes is bonded to a silicon chip with suspended LN membranes using a gold-gold bonding technique [19]. The fabrication process is outlined in Fig. 3(c). For the LN membrane chip, we begin with a chip comprising LN($300\ \text{nm}$) and SiO_2 ($5\ \mu\text{m}$) on a silicon substrate. The release windows are defined in the LN layer by patterning HSQ resist through electron-beam lithography, followed by Ar ion milling (Fig. 3(c-i)). A bonding gold layer is then deposited through a lift-off process (Fig. 3(c-ii)). Subsequently, the membrane chip is released in buffered oxide etchant (BOE) which isotropically removes the SiO_2 layer beneath. The released membrane chip is dried by a critical point dryer (CPD) (Fig. 3(c-iii)). For the electrode chip, we start with a bare sapphire substrate. We opt for sapphire due to its excellent microwave properties and transparency that aids in flip-chip alignment. Typically, the surface roughness of the bonding gold is required to be sub-nm and therefore, its thickness is controlled to be within the range of several tens of nm to

achieve the best bonding result. In this step, we deposit $40\ \text{nm}$ gold as the bonding layer. Given that this layer is thinner than the gold electrodes with $200\ \text{nm}$ thickness in our design, we compensate for the thickness difference by creating a recessed area in sapphire to accommodate the electrodes (Fig. 3(c-iv)). This step is achieved by using Cl_2 and BCl_3 plasma etching, with nickel as the hard mask. Then, $200\ \text{nm}$ -thick gold electrodes are deposited using a lift-off technique with Copolymer/PMMA resists (Fig. 3(c-v)). The nickel mask is finally removed in a piranha solution before bonding (Fig. 3(c-vi)). In the final step, we use a commercial bonding tool to bond the LN membrane chip and the electrode chip, resulting in a well-defined air gap between the membrane and electrodes (Fig. 3(c-vii)). The optical microscope image of a completed flip-chip bonded device is shown in Fig. 3(b).

RESULTS AND DISCUSSION

A ground-signal-ground (GSG) probe is employed to engage with the electrodes on the sapphire chip for measuring the non-contact resonator. The electrode pads on the sapphire chip are designed to protrude beyond the edge of the TFLN, facilitating the probe access, as

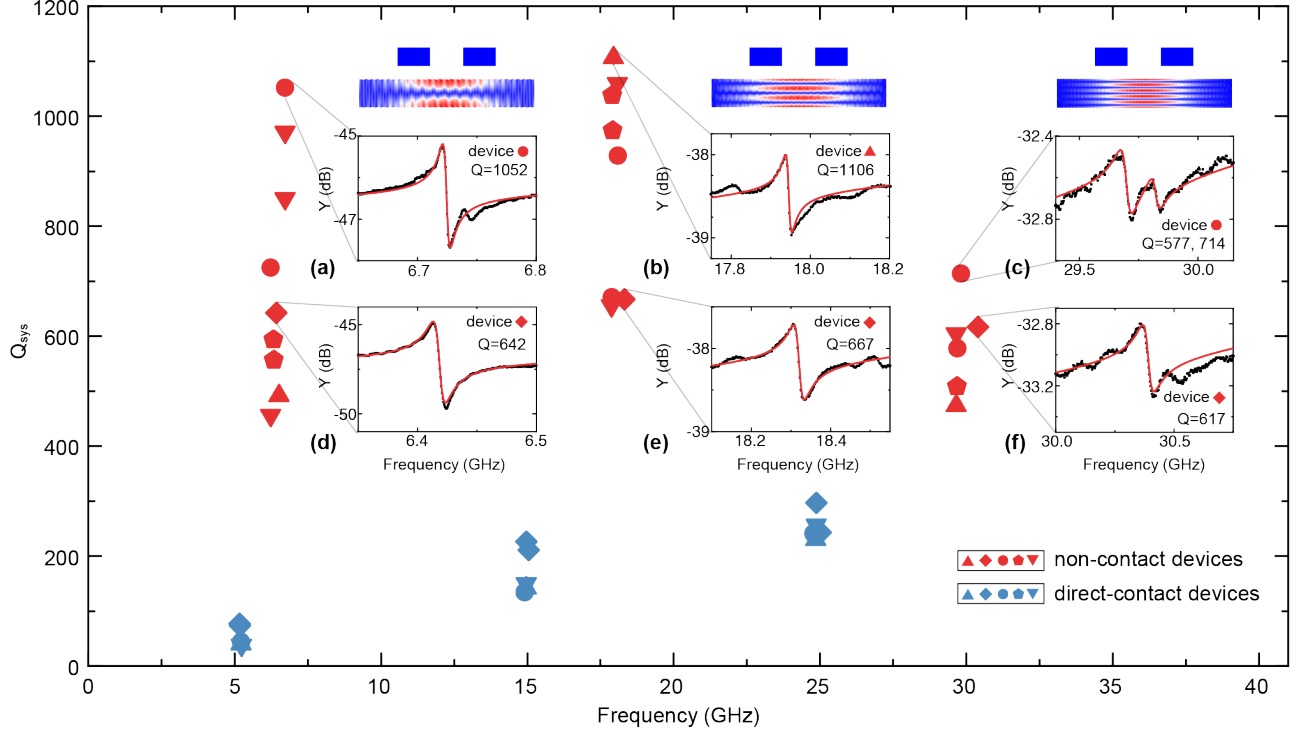


FIG. 4. Measured Q versus modal frequency for non-contact devices (red symbols, LN thickness ~ 300 nm) and direct-contact devices (blue symbols, LN thickness ~ 370 nm). Five devices from each category are marked as up-triangle, diamond, circle, pentagon and down-triangle. Insets (a-f) plot admittance spectra near the first three odd TS modes. The raw data, presented as black dots, are fitted by the mBVD model as red curves. (a-c) show the data from devices with highest Q for each mode. (d-f) represent the spectra from a chosen device (red diamond).

shown in Fig. 3(a). Via LN's piezoelectricity, the mechanical mode is coupled to the microwave field, and can be read out through a reflection measurement using a vector network analyzer.

The admittance spectra near the first three odd TS modes are plotted in the insets (a-f) of Fig. 4. A modified Butterworth-Van Dyke (mBVD) model is used to fit the experimental data [20], represented by solid lines in the insets of Fig. 4. In the mBVD model, the mechanical resonator is depicted as the combination of three lumped elements in series ($Z_{\text{mech}} = 1/(i\omega C_{\text{mech}}) + i\omega L_{\text{mech}} + R_{\text{mech}}$). In addition to exciting the resonator, two electrodes are coupled with each other, equivalent to a mutual capacitor (C_M). The mechanical Q of devices is extracted as $\sqrt{L_{\text{mech}}/C_{\text{mech}}/R_{\text{mech}}}$. The Q values of multiple mechanical resonators excited by both non-contact and direct-contact electrodes are plotted in the main graph of Fig. 4, which demonstrates significant Q enhancement of the non-contact platform. Notably, the highest experimental Q values are 1052 for TS-1 mode, 1106 for TS-3 mode and 714 for TS-5 mode, as depicted in Fig. 4(a-c). To illustrate systematic Q -improvement of the non-contact devices, we additionally plot the ad-

mittance spectra of a chosen device with average performance, as shown in Fig. 4(d-f). Remarkably, the Q values of the three modes, all exceeding 600, are still substantially higher than those observed in the direct-contact system. Therefore, despite the variations of the measured Q s in each category, it is clear that the non-contact platform systematically achieves a higher Q performance than the direct-contact case. Moreover, as indicated by the simulations in Fig. 2, this non-contact technique for enhancing the Q is universally applicable to piezoelectric materials with various loss properties.

To estimate the achieved air gap distance, we image the membrane chip using a 3D optical profilometer and observe a buckling of approximately $1.3 \mu\text{m}$ in the suspended 300 nm-thick LN film toward the silicon substrate. The extent of this buckling is consistent with the optical interference patterns observed on the suspended TFLN membrane, as shown in Fig. 3(b). The buckling of the membrane could derive from the intrinsic compressive stress of the LN films and is under further investigation. Since the resulting gap distance exceeds the designed value, the electromechanical coupling coefficients (K^2 , defined as C_{mech}/C_M) are lower than ex-

pected, measuring 0.02% and 0.01% for the TS-3 and TS-5 modes of the device represented by the red diamond symbol in Fig. 4, respectively. According to FEM simulations, if the air gap reaches 50 nm as designed, the K^2 of the non-contact case are 2.5% and 0.9% for the TS-3 and TS-5 modes, both of which are around 70% of those in the direct-contact case. Consequently, addressing the buckling in LN thin films will be a primary focus in the upcoming stages of development. The non-contact configuration with reduced buckling will deliver high performance in both achievable quality factors and K^2 characteristics.

CONCLUSIONS

We develop a flip-chip bonding technique to excite LN resonators by non-contact electrodes, resulting in notable improvement of the mechanical Q compared to the direct-contact case in the multi-GHz frequency regime (up to 30 GHz). This configuration not only effectively reduces the loss associated with the electrodes, but also holds the potential to maintain a high electromechanical coefficient. The device structure demonstrated here can be extended to other piezoelectric materials, such as AlN. With further development, the fabrication process demonstrated in this work will permit the fabrication of even thinner nanomembranes below 100 nm. These collective advantages make non-contact electromechanical resonators well-suited for high-frequency applications.

REFERENCES

-
- [1] X. Le, Q. Shi, P. Vachon, E. J. Ng, and C. Lee, Piezoelectric mems—evolution from sensing technology to diversified applications in the 5g/internet of things (iot) era, *Journal of Micromechanics and Microengineering* **32**, 014005 (2021).
 - [2] R. Weis and T. Gaylord, Lithium niobate: Summary of physical properties and crystal structure, *Applied Physics A* **37**, 191 (1985).
 - [3] M. Shen, J. Xie, C.-L. Zou, Y. Xu, W. Fu, and H. X. Tang, High frequency lithium niobate film-thickness-mode optomechanical resonator, *Applied Physics Letters* **117** (2020).
 - [4] Y. Yang, R. Lu, T. Manzanque, and S. Gong, Toward ka band acoustics: Lithium niobate asymmetrical mode piezoelectric mems resonators, in *2018 IEEE International Frequency Control Symposium (IFCS)* (IEEE, 2018) pp. 1–5.
 - [5] J. Xie, M. Shen, Y. Xu, W. Fu, L. Yang, and H. X. Tang, Sub-terahertz electromechanics, *Nature Electronics* **6**, 301 (2023).
 - [6] S. Link, R. Lu, Y. Yang, A. E. Hassanien, and S. Gong, An A1 mode resonator at 12 GHz using 160nm lithium niobate suspended thin film, in *2021 IEEE International Ultrasonics Symposium (IUS)* (2021) pp. 1–4.
 - [7] M. Faizan and L. G. Villanueva, Optimization of inactive regions of lithium niobate shear mode resonator for quality factor enhancement, *J. Microelectromech. Syst.* **30**, 369 (2021).
 - [8] Y. Yang, R. Lu, and S. Gong, High Q antisymmetric mode lithium niobate MEMS resonators with spurious mitigation, *J. Microelectromech. Syst.* **29**, 135 (2020).
 - [9] Y. Yang, L. Gao, R. Lu, and S. Gong, Lateral spurious mode suppression in lithium niobate A1 resonators, *IEEE Trans. Ultrason. Ferroelectr. Freq. Control* **68**, 1930 (2021).
 - [10] C. Tu, J. E.-Y. Lee, and X.-S. Zhang, Dissipation analysis methods and Q-Enhancement strategies in piezoelectric MEMS laterally vibrating resonators: A review, *Sensors* **20** (2020).
 - [11] H. J. Kim, S. I. Jung, J. Segovia-Fernandez, and G. Piazza, The impact of electrode materials on 1/f noise in piezoelectric AlN contour mode resonators, *AIP Adv.* **8** (2018).
 - [12] E. A. Wollack, A. Y. Cleland, P. Arrangoiz-Arriola, T. P. McKenna, R. G. Gruenke, R. N. Patel, W. Jiang, C. J. Sarabalis, and A. H. Safavi-Naeini, Loss channels affecting lithium niobate phononic crystal resonators at cryogenic temperature, *Appl. Phys. Lett.* **118** (2021).
 - [13] J. Segovia-Fernandez and G. Piazza, Thermoelastic damping in the electrodes determines Q of AlN contour mode resonators, *J. Microelectromech. Syst.* **26**, 550 (2017).
 - [14] T.-T. Yen, A. P. Pisano, and C. T.-C. Nguyen, High- Q capacitive-piezoelectric AlN lamb wave resonators, in *2013 IEEE 26th International Conference on Micro Electro Mechanical Systems (MEMS)* (2013) pp. 114–117.
 - [15] M. Carfagni, E. Lenzi, and M. Pierini, The loss factor as a measure of mechanical damping, in *Proceedings of the 16th International Modal Analysis Conference*, Vol. 3243 (1998) p. 580.
 - [16] R. Lu, Y. Yang, and S. Gong, Acoustic loss of GHz Higher-Order lamb waves in Thin-Film lithium niobate: A comparative study, *J. Microelectromech. Syst.* **30**, 876 (2021).
 - [17] T. A. Major, A. Crut, B. Gao, S. S. Lo, N. Del Fatti, F. Vallée, and G. V. Hartland, Damping of the acoustic vibrations of a suspended gold nanowire in air and water environments, *Phys. Chem. Chem. Phys.* **15**, 4169 (2013).
 - [18] R. Sandberg, K. Mølhave, A. Boisen, and W. Svendsen, Effect of gold coating on the q-factor of a resonant cantilever, *J. Micromech. Microeng.* **15**, 2249 (2005).
 - [19] E. Higurashi, K. Okumura, Y. Kunimune, T. Suga, and K. Hagiwara, Room-temperature bonding of wafers with smooth au thin films in ambient air using a surface-activated bonding method, *IEICE Trans. Electron.* **E100.C**, 156 (2017).
 - [20] J. D. Larson, P. D. Bradley, S. Wartenberg, and R. C. Ruby, Modified butterworth-van dyke circuit for fbar resonators and automated measurement system, in *2000 IEEE ultrasonics symposium. proceedings. an international symposium (Cat. No. 00CH37121)*, Vol. 1 (IEEE, 2000) pp. 863–868.

Acknowledgements

This project is supported in part by the Air Force Office of Sponsored Research (AFOSR MURI FA9550-23-1-0338) and the Defense Advanced Research Projects Agency (DARPA OPTIM HR00112320023). The part of the research that involves lithium niobate thin film preparation is supported by the US Department of Energy Co-design Center for Quantum Advantage (C2QA) under Contract No. DE-SC0012704. The authors would like to thank Yong Sun, Lauren McCabe, Kelly Woods, and Michael Rooks for their assistance provided in the device fabrication. The fabrication of the devices was done at the Yale School of Engineering & Applied Science (SEAS)

Cleanroom and the Yale Institute for Nanoscience and Quantum Engineering (YINQE).

Author contributions

H.X.T., J.X., D.W. conceived the experiment. J.X. and D.W. designed the devices. D.W. did the fabrications with contribution from Y.G., J.X. and M.S. J.X. and D.W. performed the measurement. D.W. and J.X. did simulations and processed the data with contribution from M.S.. D.W., J.X. and H.X.T. wrote the manuscript with input from all the authors. H.X.T. supervised the project.

Competing interests

The authors declare no competing interests.